MVA2005 IAPR Conference on Machine VIsion Applications, May 16-18, 2005 Tsukuba Science City, Japan
5-3

Markov Chain Monte Carlo Algorithms for 3D Ranging and Imaging

Sergio Hernández Marín
School of Engineering and Physical Sciences
Heriot Watt University
Edinburgh, EH14 4AS, UK
snh3@hw.ac.uk

Andrew M. Wallace
School of Engineering and Physical Sciences
Heriot Watt University
Edinburgh, EH14 4AS, UK
A.M.Wallace@hw.ac.uk

Gavin J. Gibson
School of Mathematical and Computer Sciences
Heriot Watt University
Edinburgh, EH14 4AS, UK
G.J.Gibson@hw.ac.uk

Abstract

We propose a new approach for the processing of Time-Correlated Single Photon Count (TCSPC) and Burst Illumination Laser (BIL) data. This data can be used to measure range, surface shape and determine a characteristic signature for remote targets. In general, the problem is to analyse the response from a histogram of either photon counts or integrated intensities to assess the number, positions and amplitudes of the reflected returns from target surfaces. The Markov chain Monte Carlo (MCMC) methodology, combined with a random sampling of the search space, enables us to detect and characterise both near and far targets from a fuller, more sensitive analysis than existing methods.

1. INTRODUCTION

In this paper we consider the processing of time-of-flight laser signals to obtain accurate range measurement and 3D reconstruction of surfaces at ranges from a few metres to several kilometres. Normally, such systems process only an assumed single return from a single opaque surface. However, we also consider situations when the laser return consists of multiple peaks, for example due to the footprint of the beam impinging on a target with surfaces distributed in depth or with semi-transparent surfaces.

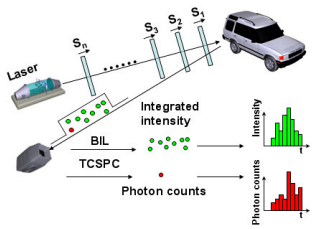

(a)

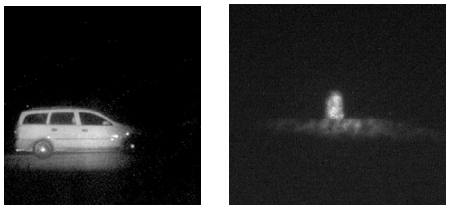

(b) (c)

Fig. 1: (a) TCSPC and BIL imaging principles. (b) Log-intensity, single frame BIL image of a car (short range). (c) Single frame BIL image of a trig point (long range).

We employ two principal approaches to range measurement and depth imaging, by Time-Correlated Single Photon Counting (TCSPC) [1], [2] and by range gating, or repeated Burst Illumination Laser (BIL) [3], [4]. With reference to Figure 1(a), a pulsed laser is directed towards the target; the time of flight (TOF) of the laser to and from the target gives a measurement of distance since the speed of light in the medium is known. However, in the TCSPC method, the detector (a single photon avalanche photodiode) records the arrival of the first photon; repeated laser pulses result in a histogram of photon arrival times that can be processed to determine the target range and signature. In the BIL method the detector (in our case an electron-bombardment CCD) integrates the received laser light over a time period (typically a few ns). Thus, the pulsed laser-CCD detector pair records the laser return from a distant slice of space. The range data is created from the multiple flashes by variable range gating. A histogram of integrated intensities is created with the time axis determined by the range gate delay.

To create a full 3D image in the TCSPC method, the laser is normally scanned but there have been advances in the development of arrays of SPADs (or geiger-mode APDs) [2], [5]. In a BIL system, the CCD records a full 2D slice in 3D space at each range gate so the 3D image is built from the repeated laser pulses as the range gate changes. The BIL images are acquired by a sensor of similar specification to that described by [4], and consist of multiple frames that have been typically acquired at thirty different range gate delays. The relative merits of each approach are discussed in the references given. It is found generally that the TCSPC approach has greater sensitivity and accuracy of measurement than the range gated method while the creation of the full 3D image is much faster in the BIL case. Figure 2 shows an example of a photon count histogram from a complex target (actually an optical system with many co-axial lens surfaces) whereas Figures 1(b) and (c) show two single frames from range gated BIL system, an estate car and trig point respectively.

Typical processing methods calculate the parameters of the distribution computing the Maximum Likelihood estimates (MLE) of a model in the frequentist framework [1]. One of the most used tools for finding the MLE is the Expectation-Maximization (EM) algorithm. This methodology fails when the number of returns increases (due to the factors mentioned in the first paragraph) and returns are occluded by the noise. Discussions about MLE and EM can be found in [6].

We use standard Markov chain Monte Carlo (MCMC), and reversible jump MCMC techniques (RJMCMC) [7] to assess the number, positions and amplitudes of the returned signals from target surfaces. The combination of these two methodologies allows moves between models with different dimensionality and within-model moves when the dimension is fixed. The main advantages of the underlying Bayesian approach of these techniques is that it provides a natural method for updating beliefs in response to new information and incorporates prior knowledge into the analysis. Furthermore, the MCMC methods provide an approximation of the full joint posterior distribution of the model parameters and therefore naturally represent the uncertainties inherent

in any inferences from the data. The goal of the work is a complete characterisation of the 3D surfaces viewed by the laser imaging system. Currently, the processing strategy is applied to single pixels or scanned elements in isolation, i.e. independently of adjacent elements in image space.

2. DATA MODELLING

The exact functional form of the photon count and the intensity histograms are unknown. In the case of the photon count histogram, we employ a nearest representation or operating model to describe the underlying distribution. This operating model is described in [8] and employs a set of four piecewise exponential functions, i.e.

$$f_{op}(i,p) = \beta \begin{cases} e^{(\frac{-(i_1-i_0)^2}{2\sigma^2})} e^{(\frac{i-i_1}{\tau_1})} & i < i_1 \\ e^{(\frac{-(i-i_0)^2}{2\sigma^2})} & i_1 \leq i < i_2 \\ e^{(\frac{-(i_2-i_0)^2}{2\sigma^2})} e^{(\frac{-(i-i_2)}{\tau_2})} & i_2 \leq i < i_3 \\ e^{(\frac{-(i_1-i_0)^2}{2\sigma^2})} e^{(\frac{-(i_3-i_2)}{\tau_2})} e^{(\frac{-(i-i_3)}{\tau_3})} & i \geq i_3 \end{cases} \quad (1)$$

where β is an amplitude factor, i_0 is the time of the peak maximum, and i_1, i_2 and i_3 are the points at which the changeovers between functions occur. We define the parameter set as follows $p = (\beta, \sigma, i_0, i_1, i_2, i_3, \tau_1, \tau_2, \tau_3)$. Assuming that, in the same histogram, several signals can be present and that these signals will be observed against a finite background level whose expected value is considered as a constant across all the channels, the observed photon histogram, $F(i,k,\Phi_{TCSPC})$, can be considered as a sample of a statistical mixture distribution with density

$$F(i,k,\Phi_{TCSPC}) = \sum_{j=1}^{k} f_{op_j}(i,p_j) + B \quad (2)$$

where *k* is the number of peaks, *B* is the background and Φ is the set of parameters of each signal and the background: $\Phi_{TCSPC} = (p_1, p_2, ..., p_k, B)$.

In this study, we assumed that the shape parameters of the returned pulses are fixed and known from an instrumental response, so the parameter set becomes $\Phi_{TCSPC} = (\boldsymbol{\beta}, \boldsymbol{i_0}, B)$, where $\boldsymbol{\beta} = (\beta_1, \beta_2, ..., \beta_k)$ and $\boldsymbol{i_0} = (i_{0_1}, i_{0_2}, ..., i_{0_k})$.

In the case of the intensity histogram, we used a look-up table of an instrumental function, $g(i)$, instead of an operating model. In practice this instrumental function is acquired from the response of the BIL system to a lambertian reflecting surface at a similar range to the object of interest. Over this distribution, only two parameters were considered: the amplitude β and the position of the peak maximum, i_0. For multiple pulses, the observed histogram equation is

$$G(i,k,\Phi_{BIL}) = \sum_{n=1}^{k} \beta_n g_n(i - i_{0_n}) \quad (3)$$

where $\Phi_{BIL} = (\boldsymbol{\beta}, \boldsymbol{i_0})$, *k* is again the number of peaks and $\boldsymbol{\beta}$ and $\boldsymbol{i_0}$ are defined as in the previous paragraph.

If the time resolution is sufficiently fine, the value x_i recorded in each channel *i* can be considered to be a random sample of a Poisson distribution with mean and variance $H(i,k,\Phi)$ which depends on the model parameters.

$$P(x_i|k,\Phi) = e^{-H(i,k,\Phi)} \frac{H(i,k,\Phi)^{x_i}}{x_i!} \quad (4)$$

Equation 4 represents the physics of sensor operation, where x_i can be either the number of photons c_i in channel *i* or the value of the intensity I_i in channel *i* and $H(i,k,\Phi)$ can be either $F(i,k,\Phi_{TCSPC})$ or $G(i,k,\Phi_{BIL})$.

3. BAYESIAN INFERENCE

In the Bayesian paradigm, the information brought by the data, the likelihood, is combined with prior information and summarised in a probability distribution called the posterior distribution, our target distribution. This posterior distribution captures knowledge about the parameters given the data. Powerful simulation algorithms, such as MCMC, allow posterior distributions, which were previously intractable, to be explored and conclusions and inferences to be drawn directly from the sampled values.

The objective of this study is inference about the unknowns *k* and Φ_{TCSPC} (respectively Φ_{BIL}) in order to obtain accurate estimates of the position, amplitude, number of peaks and background, whether required, of the returned signals. These unknowns are regarded as drawn from appropriate prior distributions. In this case, to reflect our complete prior ignorance and assuming independence of the parameters, we considered that the different parameters were drawn from different flat uniform distributions, on their respective supports:

$$\begin{array}{ll} k \sim \mathcal{U}(1, k_{\max}) & \beta_j \sim \mathcal{U}(0, \max(c_1, c_2, ..., c_{i_{\max}})) \\ i_{0_j} \sim \mathcal{U}(1, i_{\max}) & B \sim \mathcal{U}(0, (\frac{1}{i_{\max}}) \sum_{i=1}^{i_{\max}} c_i) \end{array} \quad (5)$$

The total prior distribution can be modeled as:

$$\boldsymbol{f}(k,\Phi) = f_3(B) f_4(k) \prod_{n=1}^{k} f_1(\beta_n) f_2(i_{0_n}) \quad (6)$$

where $f_r(\cdot)$, $r = \{1,2,3,4\}$, is the uniform probability density function of $(\cdot)$, which can be any parameter of the set $\{k, \beta_n, i_{0_n}, B\}$ in the respective support functions specified in equation 5.

Assuming that the photon count (intensity values) observations recorded in each channel *i* of the histogram are independent, the likelihood function can be defined using equation 4 as:

$$L(x|k,\Phi) = \prod_{i=1}^{i_{\max}} e^{-H(i,k,\Phi)} \frac{H(i,k,\Phi)^{x_i}}{x_i!} \quad (7)$$

Using equations 6 and 7 the target distribution can be expressed as:

$$\pi(k,\Phi|x) = \frac{L(x|k,\Phi)\boldsymbol{f}(k,\Phi)}{\int L(x|k,\Phi)\boldsymbol{f}(k,\Phi)d(k,\Phi)} \propto L(x|k,\Phi)\boldsymbol{f}(k,\Phi) \quad (8)$$

3.1. MCMC procedures

MCMC techniques enable simulation from an unknown distribution by embedding it as the limiting distribution of a Markov chain and simulating samples from that chain until it approaches equilibrium. When the solution space is a set of a countable number of subspaces of varying dimension, standard MCMC algorithms are not applicable and new algorithms are needed to explore all these different subspaces. The RJMCMC [7] approach copes with this problem. This is an extension of the MCMC algorithm designed to allow jumps between different dimensional spaces. This fact can be exploited to determine the suitable number of components of equations 2 and 3.

We followed a similar approach to that described in [7] where the Markov chain constructed involves moves of various types. The different moves are: (a) updates to parameters Φ,

(b) the random birth or death of a peak and (c) the random splitting of a peak into two peaks or merging of two peaks into a single peak. Let b_k be the probability of a birth or a split, and d_k the probability of a death or a merge, where *k* is the current number of peaks. Further, assume that b_k and d_k are equally probable. The following exceptions apply: 1) if the current number of peaks, *k*, is equal to 1, only a birth or a split step is allowed and 2) if the current number of peaks, *k*, is equal to a predefined maximum number of peaks, $k_{\max}$, only a death or a merge step is allowed.

The general idea of the RJMCMC technique is as follows: suppose that we have a countable family of move types $\mathcal{M}$ indexed by *m*, $m \in \mathcal{Z}^+$, and that the current state of the parameter variable set is (k, Φ), then we propose a move of type *m* to a state space (k', Φ') which is drawn from the proposal subprobability measure $q_m(k, \Phi, k', \Phi')$. The proposed move is accepted with probability $\alpha_m(k, \Phi, k', \Phi')$ given by the following general expression:

$$\alpha_m(k,\Phi,k',\Phi') = min\left\{1, \overbrace{\frac{\pi(k',\Phi'|x)}{\pi(k,\Phi|x)}}^{Target\ ratio} \times \overbrace{\frac{q_m(k',\Phi',k,\Phi)}{q_m(k,\Phi,k',\Phi')}}^{Proposal\ ratio}\right\} \tag{9}$$

3.1.1) Parameter updating: A move of type (a) is a conventional within-model step. This improves the estimate of the parameters in a state space with fixed dimension, i.e., it does not require a change of dimension of the parameter space, $k = k'$. Equation 9 reduces to the conventional Metropolis-Hastings acceptance probability given by equation 10.

$$\alpha(\Phi,\Phi') = min\left\{1, \overbrace{\frac{\pi(\Phi'|x)}{\pi(\Phi|x)}}^{Target\ ratio} \times \overbrace{\frac{q(\Phi',\Phi)}{q(\Phi,\Phi')}}^{Proposal\ ratio}\right\} \tag{10}$$

There are no restrictions on the choice of the proposal distributions. However, it is desirable to find proposal distributions that speed up the convergence of the Markov chain to its limiting distribution. Assuming independence, the proposed parameters $(\boldsymbol{\beta'}, \boldsymbol{i'_0}, B')$ were drawn from the following proposal distributions:

$$\beta' \sim \Gamma(1.5, \beta) \quad i'_0 \sim \mathcal{N}(i_0, \sigma) \quad B' \sim \Gamma(1.5, B) \tag{11}$$

where σ depends on the data (TCPSC or BIL). Therefore, the proposal distribution is:

$$q(\Phi,\Phi') = q_3(B') \prod_{j=1}^{k} q_1(\beta'_j) q_2(i'_{0_j}) \tag{12}$$

where q_1 denotes a $\Gamma(1.5, \beta_j)$ distribution, q_2 a $\mathcal{N}(i_{0_j}, \sigma)$ distribution and q_3 a $\Gamma(1.5, B)$ distribution.

3.1.2) Birth/death move: Moves (b) and (c) imply changes in the parameter-space dimensionality and therefore the reversible jump mechanism is needed. In these two specific cases the acceptance probability of equation 9 can be reduced to:

$$min\left\{1, \overbrace{\frac{\pi(k',\Phi'|x)}{\pi(k,\Phi|x)}}^{Target\ ratio} \times \overbrace{\frac{r_m(\Phi')}{r_m(\Phi)q(u)}}^{Proposal\ ratio} \times \overbrace{\left|\frac{\delta(\Phi')}{\delta(\Phi,u)}\right|}^{Jacobian}\right\} \tag{13}$$

where $r_m(x)$ is the probability of choosing move type *m* when in state Φ, *u* is a vector of continuous random variables which ensures the reversibility of the deterministic function $\Phi' = h(\Phi, u)$, which allows the move to a higher-dimensional space and *q(u)* is the probability density function of *u*. The Jacobian term joint to this deterministic function ensures the "dimension-balancing" condition which allows reversible jumps between different state spaces. The Jacobian arises from the change of variable from (Φ, u) to Φ'.

For the birth/death move we make a random choice between attempting to create a new peak or delete an existing peak with probabilities b_k and d_k. For a birth, the value of the amplitude β' and the position i'_0 of the proposed new peak are drawn from:

$$\beta' \sim \Gamma(1.5, \max(c_1, c_2, ..., c_{i_{\max}})) \quad i'_0 \sim \mathcal{U}(1, i_{\max}) \tag{14}$$

The proposal ratio is therefore:

$$\frac{d_{k+1}}{b_k} \times \{g_1(\beta') g_2(i'_0)\}^{-1} \tag{15}$$

where g_1 denotes the *gamma* probability density distribution (*pdf*) $\Gamma(1.5, \max(c_1, c_2, ..., c_{i_{\max}}))$ and g_2 denotes the *uniform pdf* $\mathcal{U}(1, i_{\max})$.

For the corresponding death move, the acceptance probability is $\min(1, (target\ ratio \times proposal\ ratio \times Jacobian)^{-1})$ with an appropriate change of index and assuming that the proposed move is a random choice between any existing peaks. For birth and death steps the determinant of the Jacobian is equal to unity.

3.1.3) Split/merge move: The split/merge move is more complicated. The choice of the deterministic function which links both moves is not straightforward since the "dimension-balancing" condition has to be verified. The random choice between split and merge uses the same probabilities b_k and d_k as in the previous case and the acceptance probability defined in equation 13.

The split proposal begins by choosing a peak, k_n, at random to split into two new peaks, k'_n and k''_n, with amplitude and position value equal to (β'_n, i'_{0_n}) and (β''_n, i''_{0_n}) respectively, conforming to equation 16

$$\begin{array}{ll} u_1 \sim \mathcal{B}e(1,1), & \Delta \sim \mathcal{U}(0, \Delta_1)\ where\ \Delta_1 = (i_3 - i_0) \\ \beta'_n = \beta_n\ u_1, & \beta''_n = \beta_n(1 - u_1) \\ i'_{0_n} = i_{0_n} - u_1\Delta, & i''_{0_n} = i_{0_n} + u_1\Delta \end{array} \tag{16}$$

The proposal ratio of equation 13 becomes:

$$\frac{d_{k+1}}{b_k} \times \{g_1(u_1) g_2(\Delta)\}^{-1} \tag{17}$$

where g_1 denotes the *Beta pdf*, $\mathcal{B}e(1,1)$, and g_2 denotes the *uniform pdf*, $\mathcal{U}(0, \Delta_1)$.

In this case the Jacobian of the transformation from $(\beta_n, i_{0_n}, u_1, \Delta)$ to $(\beta'_n, i'_{0_n}, \beta''_n, i''_{0_n})$ is not equal to one and has to be calculated.

For the merge move we choose peaks that are adjacent in terms of Δ_1, an inverted version of the splitting acceptance probability $\min(1, (target\ ratio \times proposal\ ratio \times Jacobian)^{-1})$ with the corresponding change of index and using the following parameter restructuring:

$$\beta_n = \beta'_n + \beta''_n, \quad i_{0_n} = \tfrac{i'_{0_n} + i''_{0_n}}{2} \tag{18}$$

4. RESULTS

We have applied the RJMCMC method to TCSPC LiDAR data, and the standard MCMC method to range-gated BIL data. In the former case, we have also used simulated data to provide ground truth to evaluate the accuracy of the algorithm. This shows that even when we do not have any a-priori knowledge of the dimension of the parameter space, RJMCMC is able to infer the exact number of peaks, their amplitudes and

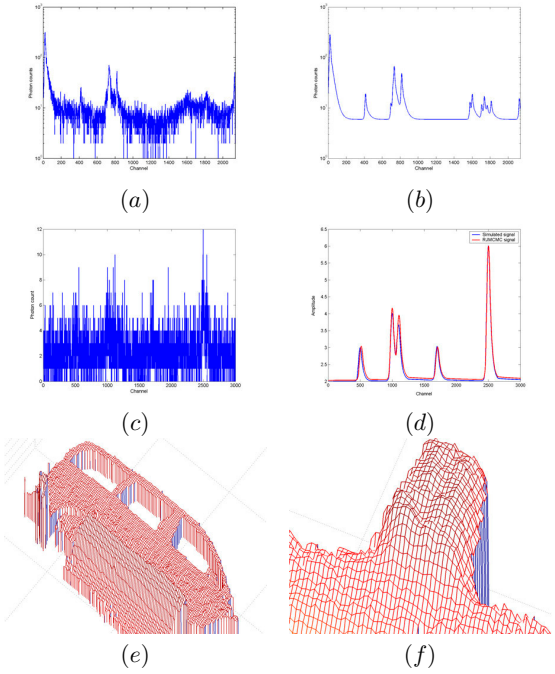

Fig. 2: (a) Histogram of photon counts (log-scale) of real data. (b) Final fit from the RJMCMC estimation of 13 returns to real data of (a). (c) Simulated signal of 5 peaks with height $\{1, 2, 1.5, 1, 4\}$ photon counts and channel position $\{500, 1000, 1100, 1700, 2500\}$ respectively against a background level of 2 counts. (d) Final fit from the RJMCMC estimation of 5 peaks to (c). The values of the height and the channel position for each peak are $\{1.009, 2.123, 1.777, 0.940, 3.954\}$ and $\{515.855, 999.599, 1106.683, 1706.952, 2501.823\}$ respectively against a background of 2.033 counts. (e) Depth image obtained with MCMC. Mesh of a car. (f) Depth image obtained with MCMC. Mesh of a trig point.

their positions. Figures 2(a) and 2(c) represent the number of detected photons (vertical axis) versus time (horizontal axis). Each recording on the vertical axis of these figures represents a single photon event. Figure 2(a) shows real data obtained from a complex target with multiple returns due to multiple and distributed or semi-transparent surfaces whereas Figure 2(c) shows a simulation of five returns using a real target signature as a model. The results obtained for these two sets of data are shown in Figures 2(b) and 2(d).

We applied the RJMCMC algorithm to the data of Figure 2(a). Then, we used the posterior mode of the marginal distribution of peaks to infer the number of peaks (in this case thirteen), see Figure 2(b). As mentioned before, in this case it is not possible to determine whether or not the number of peaks inferred is appropriate. The role of the simulated data was to establish solid basis, that is, to verify the correct working of the RJMCMC algorithm. In this case, the number of peaks and their heights and positions were known and estimations of the accuracy of the algorithm could be done. Figure 2(d) shows both the simulated signal without noise and the fitted signal obtained with RJMCMC. The overlap of both signals is almost perfect, the small variations due to the existence of noise in the original, simulated photon count histogram. Without reversible jumps, if the number of peaks is guessed incorrectly, small peaks hidden by the background or noise will be neglected.

If we believe that signal has only a single peak, we can apply the MCMC algorithm to the data. This algorithm is a special case of the RJMCMC explained in section 3 which uses only the parameter updating step of section 3.1.1. We used this methodology to evaluate whether or not it is possible to apply the Bayesian approach to evaluate BIL data. The results obtained were promising (see Figures 2(e) and (f)) but the absence of the ground truth in the experiments made impossible to determine the accuracy of the algorithm. Future experiments will be performed under laboratory conditions which will allow us to apply also the RJMCMC methodology to BIL data with multiple returns.

Figure 2(e) shows a meshed reconstruction from the BIL image sequence of a car, which is shown in Figure 1(b), acquired at a relatively short range of a few hundred metres. As can be seen in the figure, the instantaneous field of view (IFOV) is not large enough to cover all the target. On the other hand, Figure 2(f) shows a meshed reconstruction from the BIL image sequence of a trig point, which is shown in Figure 1(c), located several kilometres (far range) from the sensor. In this case, one can also see reflections from the foreground below the target.

5. Conclusions

We have described the development and application of RJMCMC techniques to process time-of-flight data using both single photon counting and variable temporal gating to extract range measurements. Our initial results show that it is possible to resolve multiple returns and hence characterise objects distributed in 3D space. We anticipate that the results obtained from processing single pixels in isolation will be improved by consideration of inter-pixel constraints imposed in the focal plane, but that remains a goal for future work.

6. Acknowledges

The authors would like to acknowledge the support of BAE SYSTEMS, the Royal Academy of Engineering and the Royal Society (Industrial Fellowship, A.M. Wallace).

References

[1] A. M. Wallace, G. S. Buller, and A. C. Walker, "3D imaging and ranging by time-correlated single photon counting," *Computing & Control Eng. Journal*, vol. 12, no. 4, pp. 157–168, 2001.

[2] M. A. Albota, R. M. Heinrichs, D. G. Kocher, *et al.*, "Three-dimensional imaging laser radar with a photon-counting avalanche photodiode array and microchip laser," *Appl. Opt.*, vol. 41, no. 36, pp. 7671–7678, 2002.

[3] J. Busck and H. Heiselberg, "Gated viewing and high-accuracy three-dimensional laser radar," *Appl. Opt.*, vol. 43, no. 24, pp. 4705–4710, 2004.

[4] R. G. Driggers, R. H. Vollmerhausen, and N. Devitt, "Impact of speckle on laser range-gated shortwave infrared imaging system target identification performance," *Opt. Eng*, vol. 42, no. 3, pp. 738–746, 2003.

[5] B. F. Aull, A. H. Loomis, D. J. Young, *et al.*, "Geiger-Mode Avalanche Photodiodes for Three-Dimensional Imaging," *Lincoln Laboratory Journal*, vol. 13, no. 2, pp. 335–348, 2002.

[6] W. R. Gilks, S. Richardson, and D. J. Spiegelhalter, *Markov chain Monte Carlo in practice*. Chapman & Hall, 1995.

[7] S. Richardson and P. J. Green, "On Bayesian analysis of mixtures with an unknown number of components," *J. Roy. Statist. Soc. Ser. B*, vol. 59, pp. 731–792, 1997.

[8] S. Pellegrini, G. S. Buller, *et al.*, "Laser-based distance measurement using picosecond resolution TCSPC," *Meas. Sci. Technol.*, vol. 11, pp. 712–716, 2000.